Gene therapy rescues photoreceptor blindness in dogs and paves the way for treating human X-linked retinitis pigmentosa

William A. Beltran[a,1], Artur V. Cideciyan[b], Alfred S. Lewin[c], Simone Iwabe[a], Hemant Khanna[d,e], Alexander Sumaroka[b], Vince A. Chiodo[f], Diego S. Fajardo[c], Alejandro J. Román[b], Wen-Tao Deng[f], Malgorzata Swider[b], Tomas S. Alemán[b], Sanford L. Boye[f], Sem Genini[a], Anand Swaroop[d,g], William W. Hauswirth[f], Samuel G. Jacobson[b], and Gustavo D. Aguirre[a,1]

[a]Section of Ophthalmology, School of Veterinary Medicine, University of Pennsylvania, Philadelphia, PA 19104; [b]Department of Ophthalmology, Scheie Eye Institute, University of Pennsylvania Perelman School of Medicine, Philadelphia, PA 19104; [c]Department of Molecular Genetics and Microbiology, University of Florida, Gainesville, FL 32610; [d]Department of Ophthalmology and Visual Sciences, University of Michigan, Ann Arbor, MI 48105; [e]Department of Ophthalmology, University of Massachusetts Medical School, Worcester, MA 01605; [f]Department of Ophthalmology, University of Florida, Gainesville, FL 32610; and [g]Neurobiology-Neurodegeneration and Repair Laboratory, National Eye Institute, National Institutes of Health, Bethesda, MD 20892

Edited by Jeremy Nathans, The Johns Hopkins University, Baltimore, MD, and approved December 20, 2011 (received for review November 16, 2011)

Hereditary retinal blindness is caused by mutations in genes expressed in photoreceptors or retinal pigment epithelium. Gene therapy in mouse and dog models of a primary retinal pigment epithelium disease has already been translated to human clinical trials with encouraging results. Treatment for common primary photoreceptor blindness, however, has not yet moved from proof of concept to the clinic. We evaluated gene augmentation therapy in two blinding canine photoreceptor diseases that model the common X-linked form of retinitis pigmentosa caused by mutations in the retinitis pigmentosa GTPase regulator (*RPGR*) gene, which encodes a photoreceptor ciliary protein, and provide evidence that the therapy is effective. After subretinal injections of adeno-associated virus-2/5–vectored human *RPGR* with human IRBP or GRK1 promoters, in vivo imaging showed preserved photoreceptor nuclei and inner/outer segments that were limited to treated areas. Both rod and cone photoreceptor function were greater in treated (three of four) than in control eyes. Histopathology indicated normal photoreceptor structure and reversal of opsin mislocalization in treated areas expressing human RPGR protein in rods and cones. Postreceptoral remodeling was also corrected: there was reversal of bipolar cell dendrite retraction evident with bipolar cell markers and preservation of outer plexiform layer thickness. Efficacy of gene therapy in these large animal models of X-linked retinitis pigmentosa provides a path for translation to human treatment.

retina | retinal degeneration

Photoreceptors function cooperatively with the retinal pigment epithelium (RPE) to optimize photon catch and generate signals that are transmitted to higher vision centers and perceived as a visual image. Disruption of the visual process in the retinal photoreceptors can result in blindness. Genetic defects in the retina cause substantial numbers of sight-impairing disorders by a multitude of mechanisms (1, 2). These genetic diseases were classically considered incurable, but the past few years have witnessed a new era of retinal therapeutics in which successful gene therapy of an animal model of one blinding human disease (3) was followed by stepwise translation to the clinic. The RPE65 form of Leber congenital amaurosis, due to a biochemical blockade of the retinoid cycle in the RPE, was the first and remains the only blinding genetic disease to be successfully treated in humans (reviewed in ref. 4).

The next level of challenge is to initiate treatment for the majority of blinding retinal disorders in which the genetic flaws are primarily in the photoreceptors. Successful targeting of therapeutic vectors to mutant photoreceptors would be required to restore function and preserve structure. Among photoreceptor dystrophies, the X-linked forms of retinitis pigmentosa (XLRP) are one of the most common causes of severe vision loss (5). More than 25 y ago, the genetic loci were identified (6), and discovery of the underlying gene defects followed (7, 8). Mutations in the retinitis pigmentosa GTPase regulator (*RPGR*) gene account for >70% of the cases of XLRP (9–11), and exon ORF15, a mutational hot spot in *RPGR*, is mutated in 22–60% of patients (12, 13). Males affected with *RPGR*-XLRP typically have night blindness in their first decade of life followed by reduction of their visual field and loss of visual acuity. By the end of their fourth decade, most patients are legally blind (14–16).

Disease-relevant animal models have been crucial in developing and validating new therapies. For *RPGR*-XLRP, there are both mouse (17–19) and canine models (20). In the dog, two naturally occurring distinct microdeletions in ORF15 result in different disease phenotypes. X-linked progressive retinal atrophy 1 [XLPRA1; deletion (del) 1,028–1,032] has a C-terminal truncation of 230 residues; the disease is juvenile, but postdevelopmental, in onset, and progresses over several years (20, 21). In contrast, the two-nucleotide deletion associated with XLPRA2 (del 1,084–1,085) causes a frameshift with inclusion of 34 basic amino acids that changes the isoelectric point of the putative protein, and truncation of the terminal 161 residues. The disease is early onset and rapidly progressive (20, 22). Both models correspond to the disease spectrum of human XLRP (5), and, although differing in relative severity, they would be equivalent to human disease occurring within the first decade of life (23).

In the present study, we used an adeno-associated virus (AAV) 2/5 vector-mediated transfer and found that gene augmentation in both rods and cones with the full-length human *RPGR*ORF15 cDNA driven by the human IRBP promoter, and, to a lesser extent by the human G-protein–coupled receptor protein kinase 1 (hGRK1) promoter, prevented photoreceptor degeneration in both canine diseases and preserved retinal structure and function.

Results

***RPGR* ORF15 Mutations Lead to Photoreceptor Degeneration in Humans and Dogs.** Topography of photoreceptors can be mapped across the retina of patients with *RPGR*-XLRP by measuring

Author contributions: W.A.B., A.V.C., S.G.J., and G.D.A. designed research; W.A.B., A.V.C., A.S.L., S.I., A. Sumaroka, A.J.R., M.S., T.S.A., S.G., A. Swaroop, W.W.H., S.G.J., and G.D.A. performed research; A.S.L., H.K., A. Sumaroka, V.A.C., D.S.F., W.-T.D., S.L.B., A. Swaroop, and W.W.H. contributed new reagents/analytic tools; W.A.B., A.V.C., A. Sumaroka, A.J.R., M.S., S.G.J., and G.D.A. analyzed data; and W.A.B., A.V.C., S.G.J., and G.D.A. wrote the paper.

Conflict of interest statement: The authors declare a conflict of interest. W.W.H. and the University of Florida have a financial interest in the use of adeno-associated virus therapies and own equity in a company (AGTC Inc.) that might, in the future, commercialize some aspects of this work. The remaining authors declare no conflict of interest.

This article is a PNAS Direct Submission.

[1]To whom correspondence may be addressed. E-mail: wbeltran@vet.upenn.edu or gda@vet.upenn.edu.

This article contains supporting information online at www.pnas.org/lookup/suppl/doi:10.1073/pnas.1118847109/-/DCSupplemental.

the thickness of the outer (photoreceptor) nuclear layer (ONL) using cross-sectional optical coherence tomography (OCT) retinal imaging (Fig. 1*A*). In normal eyes (*Inset*), ONL thickness peaks centrally and declines with distance from the fovea (24). XLRP patients with ORF15 mutations can have different disease patterns. A common pattern shows dramatic photoreceptor losses with relatively greater retention of ONL thickness at and near the cone-rich foveal region surrounded by a zone of detectable but markedly thinned ONL (Fig. 1*A*, P1). *RPGR* disease expression also includes the less common phenotype characterized by loss of central photoreceptors and diseased, yet better-preserved, peripheral photoreceptors (Fig. 1*A*, P2). The present examples, taken together with previous observations (16, 25–30), demonstrate that there can be a spectrum of human *RPGR*-XLRP phenotypes. Most of the phenotypes have more rod than cone dysfunction as measured by electroretinograms (ERGs) (30).

The two canine models can also be studied with cross-sectional retinal imaging, such as we use for human patients, and topographical photoreceptor maps can be generated and compared with normal data (Fig. 1*B*). Of translational importance is the fact that a spectrum of disease patterns also occurs in the canine models. XLPRA1 dogs, for example, can show ONL thinning with relative preservation of a region immediately superior to the optic nerve, corresponding to the high photoreceptor density of the visual streak (31). In contrast, an example of an XLPRA2 photoreceptor map shows a pattern of retina-wide ONL thinning, but more pronounced losses in the central retina, corresponding to the visual streak, than in the peripheral retina.

The natural history of photoreceptor degeneration was determined to select the age and retinal site for treatment in XLPRA1 and XLPRA2 (Fig. 1*C*). Spatiotemporal distribution of photoreceptor degeneration and the disease course were determined by quantifying ONL thickness along the vertical meridian (Fig. 1*C*). Wild-type dogs (WT) ($n = 5$, ages 7–43 wk) show a relatively uniform ONL thickness with slightly higher values (averaging 57 μm) superior to the optic nerve up to eccentricities of 35° and slightly lower values (averaging 54 μm) inferior to the optic nerve up to 25°. XLPRA1 at younger ages ($n = 7$, ages 7–28 wk) shows ONL thickness that is within or near normal limits (Fig. 1*C*). XLPRA1 at older ages ($n = 6$, ages 56–76 wk) shows ONL thinning in the inferior retina and relative preservation of the visual streak region immediately superior to the optic nerve (Fig. 1*C*, brackets). There can be greater differences among older XLPRA1 eyes, with some results near the lower limit of normal and others showing substantial ONL loss below 50% of WT (Fig. 1*C*), consistent with variable severity of disease as reported (21).

In XLPRA2 at the youngest ages examined ($n = 2$, ages 8 and 22 wk), we observed retina-wide ONL thinning that tended to be greater in the central retina (44% of WT), corresponding to the visual streak, than in the periphery (60% of WT) (Fig. 1*C*). Older XLPRA2 dogs ($n = 3$, ages 36–59 wk) show more ONL thinning with a tendency for greater central and inferior retinal disease (30% of WT) than in the superior peripheral retina (45% of WT) (Fig. 1*C*). ONL thickness in the oldest XLPRA1 and XLPRA2 eyes was substantially reduced (Fig. 1*C*).

Rod and cone retinal function in young and older dogs with XLPRA1 and XLPRA2 was measured by ERG (32). Both XLPRA1 and XLPRA2 diseases could be characterized as having more rod than cone dysfunction. Younger XLPRA1 eyes ($n = 6$) showed abnormal (4/6) rod function but normal cone function (Fig. 1*D*) whereas older XLPRA1 eyes ($n = 7$) showed abnormal rods (6/7) and cones (5/7) (Fig. 1*D*). Younger XLPRA2 eyes ($n = 3$) had abnormal rod function but mostly (2/3) normal cone function, but older XLPRA2 eyes ($n = 6$) had abnormal rod and cone function (Fig. 1*D*). Defining the differences in the structural and functional natural history of XLPRA1 and XLPRA2 diseases showed a sufficient overlap in the noninvasive studies in dogs and humans to validate the use of the dog models in proof-of-concept studies of treatment that may be relevant to *RPGR*-XLRP patients.

Treatment of XLPRA with Gene Augmentation Therapy: In Vivo Findings. Subretinal injection of the full-length human *RPGR*ORF15 cDNA under control of the hIRBP (*AAV2/5-hIRBP-hRPGR*) promoter was performed in both XLRPA1 and XLPRA2 and under control of the hGRK1 (*AAV2/5-hGRK1-hRPGR*) promoter in XLPRA2 (Table S1). In XLPRA1, treatment was initiated at 28 wk, before photoreceptor loss, and monitored to 77 wk, well after the start of degeneration (21) (Fig. 1*C*). In XLPRA2, the injections were performed at 5 wk of age, and the study terminated at 38 wk. These experiments were preceded by a series of studies with absence of rescue and some with complications (Table S2). In contrast to these treatment failures, the full-length

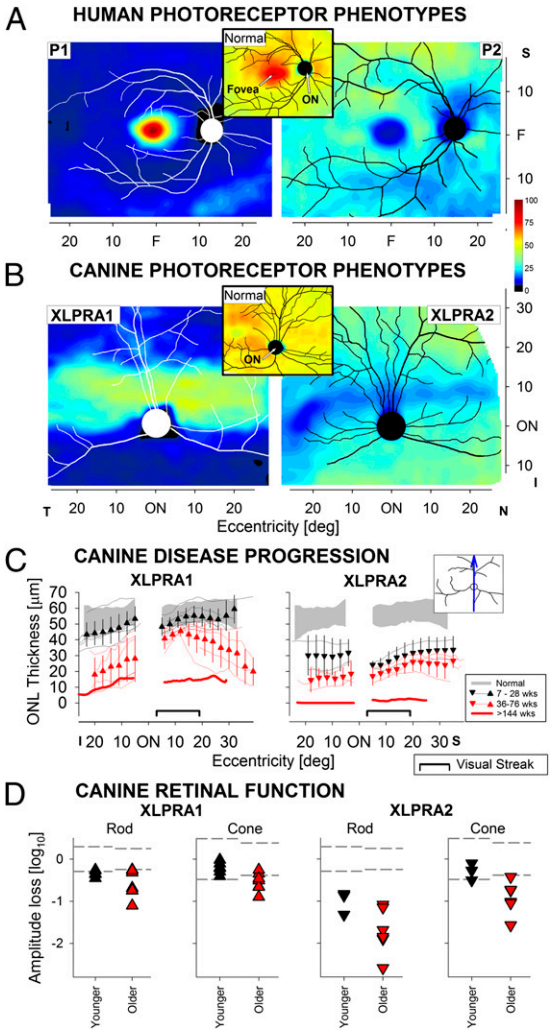

Fig. 1. Retinal disease phenotypes caused by *RPGR*ORF15 mutations in human patients and in dogs. (*A*) Different patterns of photoreceptor topography in two XLRP patients with *RPGR* mutations (P1: c.ORF15+483_484delGA, p.E746fs; P2: c.ORF15+ 652_653delAG, p.E802fs). ONL thickness topography is mapped to a pseudocolor scale. (*Inset*) Representative normal subject. Location of fovea and optic nerve (ON) are shown. (*B*) Different patterns of photoreceptor topography in the canine models of *RPGR*ORF15; mapping as performed with the human data. (*Inset*) Map of a representative WT dog with location of ON labeled. (*C*) ONL thickness profile along the vertical meridian (*Inset*) comparing XLPRA1 and XLPRA2 of different ages (thin traces) versus normal results (gray band). Mean (±SD) results are from groups of younger (7–28 wk) and older (36–76 wk) dogs. The thicker red line represents the data from the oldest dogs examined (>144 wk old). Brackets mark the location of the high photoreceptor density corresponding to the canine visual streak. (*D*) Rod and cone retinal function by ERGs in XLPRA1 (young: 7–23 wk; old: 56–80 wk) and XLPRA2 (young: 8–22 wk; old: 38–144 wk) dogs shown as the logarithm of amplitude loss from the mean WT value (rod: 2.39 and 2.38 $\log_{10}$ μV and cone: 1.50 and 1.72 $\log_{10}$ μV for younger and older, respectively). Each symbol represents an eye. Horizontal dashed lines represent the WT limits (±2 SD).

human *RPGR*ORF15 (driven by hIRBP or hGRK1 promoters) was therapeutically effective.

The positive treatment response was detectable in vivo. Treated eyes of XLPRA1 dogs had thicker ONL in the superior peripheral retina, specifically on the treated side of the subretinal injection area (bleb) boundary compared with the untreated side (Fig. 2*A*). In addition, the signal peak corresponding to the region of the photoreceptor inner and outer segments (IS/OS) was more intense and better organized on the treated side (Fig. 2*A*). Treated eyes of XLPRA2 dogs showed thicker ONL on the treated side or higher intensity signal at the level of the IS/OS (Fig. 2*A*). To understand better the relationship between the treatment bleb and local retinal structure, ONL thickness was mapped across wide expanses of the treated and control eyes (Fig. 2*B*). XLPRA1 dog H484 at 76 wk of age had a clearly demarcated zone of ONL retention within the treatment bleb in superior peripheral retina (Fig. 2*B*). There was ONL degeneration outside the bleb in the superior temporal retina. In the central retinal region where XLPRA1 dogs at this age retain near normal ONL thickness (Fig. 1*C*), a transition across the bleb boundary was less detectable (Fig. 2*B*).

XLPRA1 dog H483 with a smaller subretinal bleb had similar findings in the superior peripheral region with local evidence of ONL thickness retention inside the bleb boundary. More centrally, both treated and untreated regions retained near normal ONL thickness, and there was no change in ONL thickness corresponding to the bleb boundary (Fig. 2*B*). XLPRA2 dog Z412 showed a region with preserved ONL that corresponded to the bleb boundary; ONL was abnormally thinned outside this boundary (Fig. 2*B*). Longitudinal follow-up from 21 to 36 wk showed the time course of ONL degeneration outside the bleb of the treated eye and in the balanced salt solution (BSS)-injected control eye (Fig. S1). XLPRA2 dog Z414 showed a region of slight ONL thickness retention approximately corresponding to the bleb boundary (Fig. 2*B*).

Changes at the level of photoreceptor IS/OS were quantified. Backscatter intensity at this layer was segmented and mapped (Fig. 2*C*). IS/OS intensity maps of three of the treated dogs (H484, H483, and Z412) were similar to the ONL maps, such that regions of retained ONL corresponded to higher intensity. In the case of Z414, the treated region showed substantially higher backscatter intensity at the IS/OS layer, and this was consistent with the better layer definition apparent in individual scans (Fig. 2*A*). Comparison of the treated and BSS-injected control eyes showed the clearly delineated retinal regions with treatment-related effects (Fig. 2*C*, diagonal pattern). ERGs were evaluated in terms of interocular asymmetry (Fig. 2*D*). Signals were larger in the treated eyes of three dogs (H484, Z412, and Z414) for photoreceptor responses dominated by rods and for postreceptoral bipolar cell responses mediated by both rods and cones. H483 had the least degenerate retina and normal amplitude responses bilaterally (Fig. 2*D* and Fig. S2) that were symmetric for cones and asymmetric for rods, favoring the untreated eye.

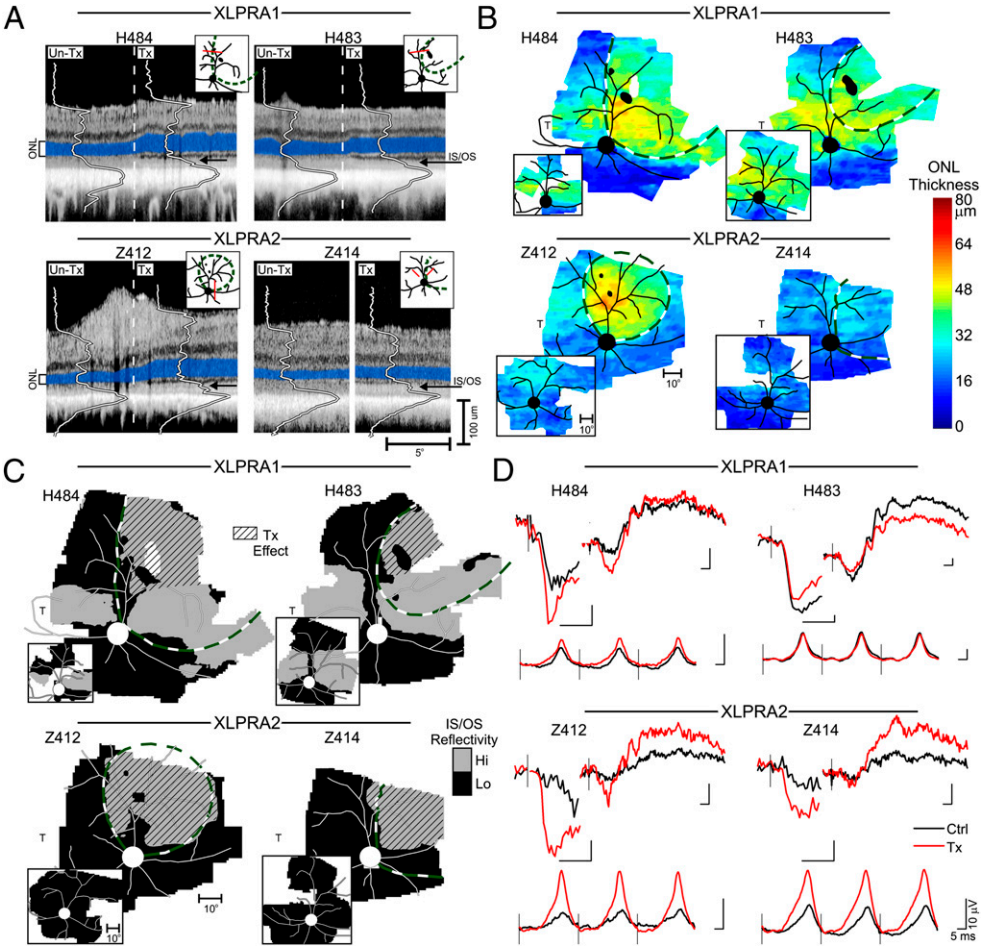

Fig. 2. In vivo evidence of gene augmentation therapy success in XLPRA dogs. (*A*) Cross-sectional OCT retinal scans crossing the treatment bleb boundary (dashed line in H484, H483, and Z412) or comparing inside and outside the bleb region (white space in Z414) in treated eyes of XLPRA1 (H484, H483) and XLPRA2 (Z412, Z414) dogs. ONL is highlighted in blue for visibility. Overlaid are the longitudinal reflectivity profiles defining the backscattered light intensity from different retinal layers. Arrows point to the backscatter peak originating from the IS/OS region. (*Insets*) Red line represents the location of the scans. (*B*) Topography of ONL thickness in treated eyes shown on a pseudocolor scale with superimposed retinal blood vessels and optic nerve. White represents no data; irregularly shaped black foci indicate retinotomy sites. Bleb boundaries are outlined with green-and-white dashed lines. Small inset figures are BSS-treated control fellow eyes. (*C*) Topography of average backscatter intensity originating from the photoreceptor IS/OS region in treated eyes with superimposed retinal blood vessels and optic nerve. The same threshold is used in all eyes to distinguish regions of high (gray) and low (black) IS/OS backscatter. Diagonal-pattern regions delineate the treatment effect by comparison of the two eyes. All eyes are shown as equivalent right eyes for comparability. T, temporal retina. (*B* and *C*) (*Insets*) BSS-treated contralateral eyes. (*D*) ERGs in treated (red traces) and BSS-injected control fellow eyes (black traces). For each panel in *D*, the upper-left waveforms are the leading edges of the photoresponses driven by rod photoreceptor activation, and the upper-right waveforms are the b-waves dominated by rod bipolar cells, both recorded under dark-adapted conditions. Lower waveforms are 29-Hz flicker responses dominated by cone function recorded under light-adapted conditions. Black vertical lines show the timing of flash onset. Calibrations are 5 ms (abscissa) and 10 µV (ordinate); note the ~3× larger waveforms of H483.

Gene Augmentation Rescues Photoreceptors and Reverses Mislocalization of Rod and Cone Opsins in Both XLPRA Genotypes. Assessment of retinal morphology in tissue sections that included the bleb boundary confirmed the in vivo imaging results of retention of ONL thickness and photoreceptor preservation in subretinally-treated areas (Fig. 3, panels 1–5; Fig. S3). Intravitreal vector administration was comparable to no treatment (Table S1). In the three dogs treated with *AAV2/5-hIRBP-hRPGR* (H484, H483, Z412), rod and cone IS and OS structure was normal within the bleb boundary. In the untreated areas, IS were short and OS were sparse and irregular (Fig. 3, panels 3 and 4; Fig. S3). In Z414, treated with *AAV2/5-hGRK1-hRPGR*, a milder yet positive photoreceptor rescue was observed in the bleb area (Fig. S3*C*). Immunolabeling with an antibody directed against human RPGRORF15 (33) detected robust hRPGR protein expression limited to photoreceptors in the treatment area (Table S1). Labeling was found throughout the IS and synaptic terminals in the four dogs, as well as in the rod and cone perinuclear region of H484 (Fig. 3, panels 6–8; Fig. S3). Finally, the mislocalization of rod and cone opsins, a feature of the disease in human (34), mouse (17), and dog (22, 35), was reversed (Fig. 3, panels 9, 10, 12, and 13; Fig. S3) in the three dogs treated with *AAV2/5-hIRBP-hRPGR*. Reduced yet distinct rod and red/green (R/G) cone opsin mislocalization was apparent in Z414 treated with *AAV2/5-hGRK1-hRPGR* (Fig. S3*C*).

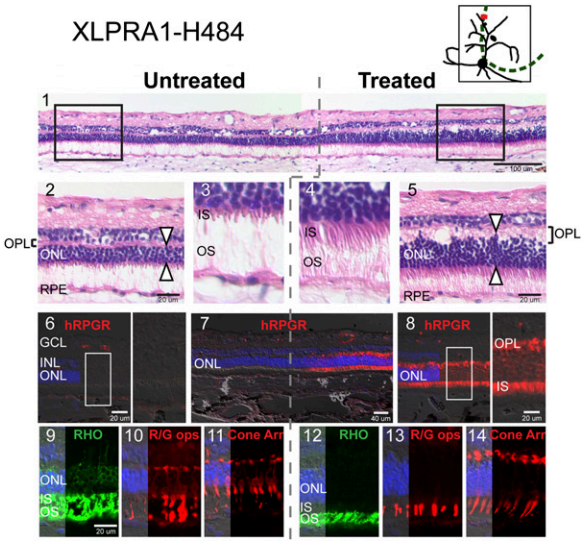

Fig. 3. Gene augmentation therapy rescues photoreceptors in the XLPRA1 dog H484 treated with *AAV2/5-hIRBP-hRPGR* at 28 wk of age and terminated at 77 wk. The schematic drawing illustrates the treatment area (dashed green lines) and the location of the region (red line) illustrated in the section. (1) Representative H&E-stained cryosection at the nontreated/treated junction (vertical dashed line). Boxed areas are illustrated at higher magnification below (2–5). Photoreceptor density is decreased in nontreated region and both ONL (white arrowheads) and OPL are narrowed; rod and cone IS are short, and OS sparse. In treated regions, the number of photoreceptors is increased and their structure is normal (4 and 5), resulting in thicker ONL and preserved OPL. (6–8) Expression of hRPGRORF15 in treated areas decreases in the transition zone and is absent elsewhere. Protein is present in rod and cone inner segments and synaptic regions and, to a lesser extent, in the perinuclear cytoplasm where expression is most intense. (9, 10, 12, and 13) Rod (RHO) and red/green cone (R/G ops) opsins are mislocalized in untreated regions with label in the IS, ONL, and synaptic terminals. Treated areas show normal localization to the OS. (11 and 14) Preservation of normal cone structure in treated areas is clearly shown with cone arrestin (Cone Arr) labeling. GCL, ganglion cell layer; INL, inner nuclear layer; IS, inner segments; ONL, outer nuclear layer; OPL, outer plexiform layer; OS, outer segments; RPE, retinal pigment epithelium.

Prevention of Secondary OPL, Bipolar Cell, and Inner Retinal Disease. In XLPRA, as in other primary photoreceptor diseases, OPL and inner retinal abnormalities are common secondary effects (22, 35–37). In untreated regions, narrowing of the OPL was associated with compressed photoreceptor synaptic terminals (Fig. 3, panels 2 and 5; Fig. S3) and with a reduction of the number of CtBP2-labeled synaptic ribbons in rod and cone terminals (Fig. 4, panels 1 and 2; Fig. S4). In parallel, rod and cone bipolar cell dendrites retracted (Fig. 4, panels 3 and 4; Fig. S4). These secondary changes were absent in treated areas, resulting in a preserved OPL. In contrast, calbindin labeling of horizontal and amacrine cells (Fig. 4, panels 5 and 6; Fig. S4) and their lateral processes was normal and unchanged between treated and untreated regions. These last-mentioned hallmarks, however, are of late-stage retinal remodeling in XLPRA (22, 35) and were not expected to be present at the age when dogs were terminated.

The dendritic terminals of horizontal cells, as well as those of ganglion cells, and the nerve fiber layer of treated and untreated regions appeared normal when labeled with an antibody directed against the neurofilament heavy chain (NF200 kDa). However, there was punctate NF200 staining in the ONL. Overexpression of neurofilaments is a characteristic of axonal injury in several neurodegenerative disorders and occurs in this and other retinal diseases (38). This finding was restricted to the untreated regions of all dogs and was absent or reduced in treated areas (Fig. 4, panels 5 and 6; Fig. S4). GFAP immunolabeling clearly delineated untreated regions that showed increased Müller glia reactivity, whereas labeling diminished in the transition zone between treated and untreated regions and was absent in the bleb area (Fig. 4, panels 7 and 8; Fig. S4). In summary, inner retinal rescue was complete in three of four treated eyes; rescue

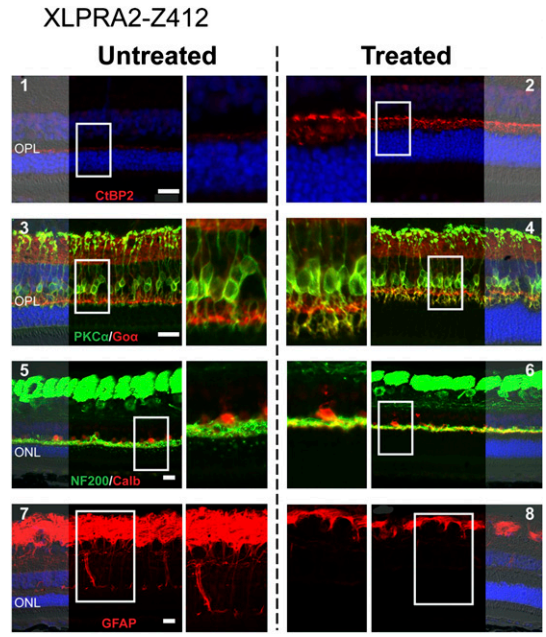

Fig. 4. Successful gene therapy rescues retinal remodeling in the XLPRA2 dog Z412 treated with *AAV2/5-hIRPB-hRPGR* at 5 wk of age and terminated at 38 wk. Immunolabeling with CtBP2/RIBEYE shows a reduced number of photoreceptor synaptic ribbons in the untreated areas (1). In treated areas, the density of synaptic ribbons is normal, thus contributing to the preservation of the OPL thickness (2). Coimmunolabeling of rod bipolar (PKCα) and ON bipolar cells (Goα) shows retraction of dendrites in untreated areas (3), whereas dendritic arborization is preserved in treated regions (4). (5 and 6) Coimmunolabeling of the inner retina with antibodies to neurofilament 200 kDa (NF200) and calbindin (Calb) is normal in both untreated and treated regions, but punctate NF200 staining is seen in the ONL in untreated areas. (7 and 8) GFAP immunolabeling of Müller cell radial extensions is found only in untreated areas, whereas no reactive Müller cells are seen in the treated regions.

was partial for the eye treated with *AAV2/5-hGRK1-hRPGR* where rod neurite sprouting extended into the inner retina (Table S1), and the NF200 labeling pattern was intermediate between normal and disease (Fig. S4*C*). The results clearly show that targeting *RPGR* augmentation to photoreceptors in both XLPRA1 and XLPRA2 corrects the primary photoreceptor defect and has beneficial downstream effects as OPL and inner retinal abnormalities are prevented or reversed.

Discussion

Recent successes using gene replacement to treat LCA2, the autosomal recessive RPE disease due to *RPE65* mutations, have paved the way for considering gene therapy for treating other incurable human retinopathies (reviewed in refs. 4 and 39). XLRP is among the candidate diseases for treatment because it can be identified in the clinic through pedigree analysis, carrier identification, or by the fact that there is a high frequency of XLRP among simplex males with retinitis pigmentosa (13), and mutations in *RPGR*ORF15 account for about 75% of XLRP patients (40). The current results showing treatment efficacy in two large animal models of human *RPGR*ORF15-XLRP strongly suggest that a gene augmentation strategy is a viable option for this photoreceptor ciliopathy and complements successful rod rescue in a murine model of the Bardet–Biedl syndrome ciliopathy (41).

The disease in humans and in animal models is not, however, without complexity, and future therapy of the human disease will need to be approached with caution. For example, there are modifiers that may affect disease expression in both patients and dog models (30, 42), and there is a spectrum of phenotypes between and within *RPGR*-XLRP families (28) and in the dog XLPRA1 model (21). The phenotypic diversity may be a potential obstacle to patient selection and also points to the need for more than a molecular diagnosis and the patient's age as criteria to determine candidacy for treatment. In support of genotype data, there must be complementing, detailed, noninvasive retinal imaging and function studies. The temptation should be resisted in early human treatment approaches to try to design a treatment to fit all phenotypes and all disease stages. The dog diseases are mainly rod > cone degenerations, and there was efficacy in treating both the severe XLPRA2 with central retinal degeneration and the less severe XLPRA1 with central retinal preservation using vectors that targeted both rods and cones. Not included in the canine disease spectrum, however, are certain human *RPGR*-XLRP phenotypes, such as mild cone > rod or cone dystrophies (25, 26, 43–45). Some patients can show very limited or even normal rod function, and cone-targeting strategies must be developed for these subtypes. Proof-of-principle studies targeting cone diseases already have been successful in both mouse and dog models with mutations in cone phototransduction (46) or cyclic GMP gated channel (47–49) genes, allowing translation to the clinic to be expedited.

The reported intrafamilial variation of phenotypes (28) neither excludes nor includes entire pedigrees from participation, but further strengthens the case for complete clarification of phenotype in individual patients. Furthermore, in the present study, there was no attempt to target the very central retina; the extracentral subretinal approach as used in the dogs would be the advisable strategy for early phase human clinical trials on the basis of the current observations. However, many *RPGR* patients show continued survival of foveal cones and impaired but useful visual acuity in late disease stages (15). Because subfoveal injections of viral vector constructs have been shown to cause loss of diseased foveal cones (50), an alternate means of therapeutic gene delivery should be considered. Advances in intravitreal delivery systems to treat the outer retina, for example, using mutant AAV capsid vectors (51), eventually could allay the safety concerns in treating residual foveal cones.

Although it is clear that *RPGR*-associated disease is common and generally severe, the function of the gene, and the association between mutation and disease, are less well understood. *RPGR* has a complex splicing pattern with multiple tissue- and cell-specific isoforms (52), is known to interact with a number of ciliary proteins (53, 54), acts as a gunanine nucleotide exchange factor for small GTPase RAB8A (55), and may have a role in vertebrate development (56). Such complexity may account partially for the variability in disease phenotype. In general, loss-of-function (13, 17) or gain-of-function (19, 20, 22) mechanisms have been proposed (56), suggesting that each would require different therapeutic approaches. Although our present studies cannot rule out either mechanism as causal to disease, the results clearly indicate that gene augmentation alone is effective in preventing disease or in arresting and reversing the degenerative process in canine models of ORF15 mutations. These fundamental findings allow us to move forward therapeutically toward translational studies while the specific disease mechanisms await further elucidation.

Our results emphasize that targeting therapy to rod and cone photoreceptors is essential for functional and structural rescue in *RPGR*-associated retinal disease. The hIRBP promoter that regulates expression of the therapeutic gene results in robust expression of reporter or therapeutic genes in both cell types (Fig. S5; Fig. 3, panels 6–8; Fig. S3), and expression is sustained. As IRBP also is expressed in human cones (57), we expect efficient targeting of rods and cones with this promoter in future translational studies. When regulated by the hGRK1 promoter, the therapeutic transgene expression was low in rods and, to a lesser extent, in cones. The remaining photoreceptor structure, albeit abnormal, was considerably improved over untreated regions.

In XLPRA1, treatment before disease onset prevented disease development. Furthermore, treatment of XLPRA2 after disease onset, and while photoreceptor cell death was ongoing [at 5 wk, cell death is ~50% of the maximal rate determined by TUNEL labeling (22)], arrested progression of the disease, and the morphology of the remaining photoreceptors was restored to normal. At least for the stages of disease studied, this therapeutic vector was highly effective and warrants further studies for translational applications. In both models, treatment with the *hIRPB-hRPGR* therapeutic vector prevented (XLPRA1) or reversed (XLPRA2) rod and R/G cone opsin mislocalization, a feature of the disease in human (34), mouse (17), and dog (22, 35) and a putative early marker of photoreceptor cell death (58, 59).

A characteristic feature of photoreceptor degenerations is progressive changes in the OPL, bipolar cells, and inner retinal layers (22, 35–37). These were widespread in untreated areas, but reversed to normal in treated areas, particularly when the *AAV2/5-hIRPB-hRPGR* vector was used. Prevention of remodeling occurred when XLPRA1 retinas were treated before disease onset, whereas, in XLPRA2, early OPL synaptic changes, bipolar cell abnormalities, and inner retinal abnormalities were abrogated with treatment, and normal structure ensued. Thus, treatment of the primary photoreceptor defect has beneficial downstream effects as OPL and inner retinal abnormalities are prevented or reversed. This may account for the improved postreceptoral responses recorded from three of the four treated dogs. Future studies should extend the posttreatment follow-up period to older ages when degeneration of untreated regions would allow testing of treatment consequences at the visual brain such as with the use of pupillometry and visual evoked potentials, and ultimately with visual behavior.

Subretinal treatment in XLPRA canine models of *RPGR*ORF15-XLRP with AAV2/5 vectors and the full-length human *RPGR*ORF15 cDNA was effective in preserving photoreceptor structure and function. The treatment was more effective when the hIRBP promoter regulated the therapeutic transgene rather than the hGRK1 promoter; however, we acknowledge that a much larger sample size is necessary to make a definitive conclusion. The success of this therapeutic approach emphasizes the need for further development of this therapy and paves the way for treating the *RPGR* form of human retinitis pigmentosa.

Materials and Methods

Patients with XLRP and molecularly confirmed *RPGR*ORF15 mutations were included in this study for retinal cross-sectional imaging. XLPRA1 and XLPRA2 dogs were subretinally injected with an AAV2/5 vector carrying a full-length human *RPGR*ORF15 cDNA under the control of either a human IRBP or GRK1 promoter. Assessment of the response to gene transfer was made by means of clinical ophthalmic examinations, *en face* and cross-

NEUROSCIENCE

sectional in vivo retinal imaging, electroretinography, and morphological evaluation on retinal histological sections. Methodological details are provided in *SI Materials and Methods*.

ACKNOWLEDGMENTS. We thank Svetlana Savina for help with immunohistochemistry, Karla Carlisle and the Retinal Disease Studies Facility staff for animal care, Lydia Melnyk for research coordination, Dr. Muayyad al-Ubaidi for the human IRBP promoter plasmid, and Dr. Cheryl Craft for the human cone arrestin antibody. This work was supported by National Institutes of Health Grants EY-06855, EY-17549, EY-007961, EY-021721, P30 EY-001583, and 2PNEY018241, the Foundation Fighting Blindness, a Fight for Sight Nowak family grant, the Midwest Eye Banks and Transplantation Center, the Macula Vision Research Foundation, the Van Sloun Fund for Canine Genetic Research, and Hope for Vision.

1. Wright AF, Chakarova CF, Abd El-Aziz MM, Bhattacharya SS (2010) Photoreceptor degeneration: Genetic and mechanistic dissection of a complex trait. *Nat Rev Genet* 11:273–284.
2. Bramall AN, Wright AF, Jacobson SG, McInnes RR (2010) The genomic, biochemical, and cellular responses of the retina in inherited photoreceptor degenerations and prospects for the treatment of these disorders. *Annu Rev Neurosci* 33:441–472.
3. Acland GM, et al. (2001) Gene therapy restores vision in a canine model of childhood blindness. *Nat Genet* 28:92–95.
4. Cideciyan AV (2010) Leber congenital amaurosis due to RPE65 mutations and its treatment with gene therapy. *Prog Retin Eye Res* 29:398–427.
5. Bird AC (1975) X-linked retinitis pigmentosa. *Br J Ophthalmol* 59:177–199.
6. Bhattacharya SS, et al. (1984) Close genetic linkage between X-linked retinitis pigmentosa and a restriction fragment length polymorphism identified by recombinant DNA probe L1.28. *Nature* 309:253–255.
7. Meindl A, et al. (1996) A gene (RPGR) with homology to the RCC1 guanine nucleotide exchange factor is mutated in X-linked retinitis pigmentosa (RP3). *Nat Genet* 13:35–42.
8. Schwahn U, et al. (1998) Positional cloning of the gene for X-linked retinitis pigmentosa 2. *Nat Genet* 19:327–332.
9. Bader I, et al. (2003) X-linked retinitis pigmentosa: *RPGR* mutations in most families with definite X linkage and clustering of mutations in a short sequence stretch of exon ORF15. *Invest Ophthalmol Vis Sci* 44:1458–1463.
10. Sharon D, et al. (2003) RP2 and RPGR mutations and clinical correlations in patients with X-linked retinitis pigmentosa. *Am J Hum Genet* 73:1131–1146.
11. Pelletier V, et al. (2007) Comprehensive survey of mutations in RP2 and RPGR in patients affected with distinct retinal dystrophies: Genotype-phenotype correlations and impact on genetic counseling. *Hum Mutat* 28:81–91.
12. Vervoort R, et al. (2000) Mutational hot spot within a new RPGR exon in X-linked retinitis pigmentosa. *Nat Genet* 25:462–466.
13. Breuer DK, et al. (2002) A comprehensive mutation analysis of RP2 and RPGR in a North American cohort of families with X-linked retinitis pigmentosa. *Am J Hum Genet* 70:1545–1554.
14. Jacobson SG, et al. (1997) Disease expression in X-linked retinitis pigmentosa caused by a putative null mutation in the RPGR gene. *Invest Ophthalmol Vis Sci* 38: 1983–1997.
15. Sandberg MA, Rosner B, Weigel-DiFranco C, Dryja TP, Berson EL (2007) Disease course of patients with X-linked retinitis pigmentosa due to RPGR gene mutations. *Invest Ophthalmol Vis Sci* 48:1298–1304.
16. Aleman TS, et al. (2007) Inner retinal abnormalities in X-linked retinitis pigmentosa with RPGR mutations. *Invest Ophthalmol Vis Sci* 48:4759–4765.
17. Hong DH, et al. (2000) A retinitis pigmentosa GTPase regulator (RPGR)-deficient mouse model for X-linked retinitis pigmentosa (RP3). *Proc Natl Acad Sci USA* 97: 3649–3654.
18. Chang B, et al. (2002) Retinal degeneration mutants in the mouse. *Vision Res* 42: 517–525.
19. Hong DH, Pawlyk BS, Adamian M, Li T (2004) Dominant, gain-of-function mutant produced by truncation of RPGR. *Invest Ophthalmol Vis Sci* 45:36–41.
20. Zhang Q, et al. (2002) Different RPGR exon ORF15 mutations in Canids provide insights into photoreceptor cell degeneration. *Hum Mol Genet* 11:993–1003.
21. Zeiss CJ, Acland GM, Aguirre GD (1999) Retinal pathology of canine X-linked progressive retinal atrophy, the locus homologue of RP3. *Invest Ophthalmol Vis Sci* 40: 3292–3304.
22. Beltran WA, Hammond P, Acland GM, Aguirre GD (2006) A frameshift mutation in RPGR exon ORF15 causes photoreceptor degeneration and inner retina remodeling in a model of X-linked retinitis pigmentosa. *Invest Ophthalmol Vis Sci* 47:1669–1681.
23. Wright AF, et al. (2004) Lifespan and mitochondrial control of neurodegeneration. *Nat Genet* 36:1153–1158.
24. Jacobson SG, et al. (2011) Human retinal disease from AIPL1 gene mutations: Foveal cone loss with minimal macular photoreceptors and rod function remaining. *Invest Ophthalmol Vis Sci* 52:70–79.
25. Ayyagari R, et al. (2002) X-linked recessive atrophic macular degeneration from RPGR mutation. *Genomics* 80:166–171.
26. Ebenezer ND, et al. (2005) Identification of novel RPGR ORF15 mutations in X-linked progressive cone-rod dystrophy (XLCORD) families. *Invest Ophthalmol Vis Sci* 46: 1891–1898.
27. Shu X, et al. (2007) RPGR mutation analysis and disease: An update. *Hum Mutat* 28: 322–328.
28. Walia S, et al. (2008) Discordant phenotypes in fraternal twins having an identical mutation in exon ORF15 of the RPGR gene. *Arch Ophthalmol* 126:379–384.
29. Ruddle JB, et al. (2009) RPGR ORF15 genotype and clinical variability of retinal degeneration in an Australian population. *Br J Ophthalmol* 93:1151–1154.
30. Fahim AT, et al. (2011) Allelic heterogeneity and genetic modifier loci contribute to clinical variation in males with X-linked retinitis pigmentosa due to RPGR mutations. *PLoS ONE* 6:e23021.
31. Mowat FM, et al. (2008) Topographical characterization of cone photoreceptors and the area centralis of the canine retina. *Mol Vis* 14:2518–2527.
32. Acland GM, et al. (2005) Long-term restoration of rod and cone vision by single dose rAAV-mediated gene transfer to the retina in a canine model of childhood blindness. *Mol Ther* 12:1072–1082.
33. Khanna H, et al. (2005) RPGR-ORF15, which is mutated in retinitis pigmentosa, associates with SMC1, SMC3, and microtubule transport proteins. *J Biol Chem* 280: 33580–33587.
34. Adamian M, Pawlyk BS, Hong DH, Berson EL (2006) Rod and cone opsin mislocalization in an autopsy eye from a carrier of X-linked retinitis pigmentosa with a Gly436Asp mutation in the RPGR gene. *Am J Ophthalmol* 142:515–518.
35. Beltran WA, Acland GM, Aguirre GD (2009) Age-dependent disease expression determines remodeling of the retinal mosaic in carriers of RPGR exon ORF15 mutations. *Invest Ophthalmol Vis Sci* 50:3985–3995.
36. Aguirre GD, et al. (2002) Retinal histopathology of an XLRP carrier with a mutation in the RPGR exon ORF15. *Exp Eye Res* 75:431–443.
37. Li ZY, Kljavin IJ, Milam AH (1995) Rod photoreceptor neurite sprouting in retinitis pigmentosa. *J Neurosci* 15:5429–5438.
38. Geiger K, et al. (1994) Transgenic mice expressing IFN-gamma in the retina develop inflammation of the eye and photoreceptor loss. *Invest Ophthalmol Vis Sci* 35: 2667–2681.
39. Jacobson SG, Cideciyan AV (2010) Treatment possibilities for retinitis pigmentosa. *N Engl J Med* 363:1669–1671.
40. Wright AF, Shu X (2007) Focus on Molecules: RPGR. *Exp Eye Res* 85:1–2.
41. Simons DL, Boye SL, Hauswirth WW, Wu SM (2011) Gene therapy prevents photoreceptor death and preserves retinal function in a Bardet-Biedl syndrome mouse model. *Proc Natl Acad Sci USA* 108:6276–6281.
42. Guyon R, Pearce-Kelling SE, Zeiss CJ, Acland GM, Aguirre GD (2007) Analysis of six candidate genes as potential modifiers of disease expression in canine XLPRA1, a model for human X-linked retinitis pigmentosa 3. *Mol Vis* 13:1094–1105.
43. Demirci FY, et al. (2002) X-linked cone-rod dystrophy (locus COD1): Identification of mutations in RPGR exon ORF15. *Am J Hum Genet* 70:1049–1053.
44. Yang Z, et al. (2002) Mutations in the RPGR gene cause X-linked cone dystrophy. *Hum Mol Genet* 11:605–611.
45. Demirci FY, et al. (2005) Histopathologic study of X-linked cone-rod dystrophy (CORDX1) caused by a mutation in the RPGR exon ORF15. *Am J Ophthalmol* 139: 386–388.
46. Alexander JJ, et al. (2007) Restoration of cone vision in a mouse model of achromatopsia. *Nat Med* 13:685–687.
47. Komáromy AM, et al. (2010) Gene therapy rescues cone function in congenital achromatopsia. *Hum Mol Genet* 19:2581–2593.
48. Michalakis S, et al. (2010) Restoration of cone vision in the CNGA3-/- mouse model of congenital complete lack of cone photoreceptor function. *Mol Ther* 18:2057–2063.
49. Carvalho LS, et al. (2011) Long-term and age-dependent restoration of visual function in a mouse model of CNGB3-associated achromatopsia following gene therapy. *Hum Mol Genet* 20:3161–3175.
50. Jacobson SG, et al. (2012) Gene therapy for Leber congenital amaurosis caused by RPE65 mutations: Safety and efficacy in 15 children and adults followed up to 3 years. *Arch Ophthalmol* 130:9–24.
51. Petrs-Silva H, et al. (2011) Novel properties of tyrosine-mutant AAV2 vectors in the mouse retina. *Mol Ther* 19:293–301.
52. He S, et al. (2008) Retinitis pigmentosa GTPase regulator (RPGR) protein isoforms in mammalian retina: Insights into X-linked retinitis pigmentosa and associated ciliopathies. *Vision Res* 48:366–376.
53. Murga-Zamalloa CA, Desai NJ, Hildebrandt F, Khanna H (2010) Interaction of ciliary disease protein retinitis pigmentosa GTPase regulator with nephronophthisis-associated proteins in mammalian retinas. *Mol Vis* 16:1373–1381.
54. Shu X, et al. (2005) RPGR ORF15 isoform co-localizes with RPGRIP1 at centrioles and basal bodies and interacts with nucleophosmin. *Hum Mol Genet* 14:1183–1197.
55. Murga-Zamalloa CA, Atkins SJ, Peranen J, Swaroop A, Khanna H (2010) Interaction of retinitis pigmentosa GTPase regulator (RPGR) with RAB8A GTPase: Implications for cilia dysfunction and photoreceptor degeneration. *Hum Mol Genet* 19:3591–3598.
56. Ghosh AK, et al. (2010) Human retinopathy-associated ciliary protein retinitis pigmentosa GTPase regulator mediates cilia-dependent vertebrate development. *Hum Mol Genet* 19:90–98.
57. Porrello K, Bhat SP, Bok D (1991) Detection of interphotoreceptor retinoid binding protein (IRBP) mRNA in human and cone-dominant squirrel retinas by in situ hybridization. *J Histochem Cytochem* 39:171–176.
58. Alfinito PD, Townes-Anderson E (2002) Activation of mislocalized opsin kills rod cells: A novel mechanism for rod cell death in retinal disease. *Proc Natl Acad Sci USA* 99: 5655–5660.
59. Zhang T, Zhang N, Baehr W, Fu Y (2011) Cone opsin determines the time course of cone photoreceptor degeneration in Leber congenital amaurosis. *Proc Natl Acad Sci USA* 108:8879–8884.

Supporting Information

Beltran et al. 10.1073/pnas.1118847109

SI Materials and Methods

Human Subjects and Retinal Cross-Sectional Imaging. Patients with XLRP and molecularly confirmed *RPGR*ORF15 mutations were included in this study. Informed consent was obtained. Procedures followed the Declaration of Helsinki guidelines and were approved by the institutional review board. Retinal cross-sectional imaging was obtained with spectral-domain optical coherence tomography (SD-OCT, RTVue-100; Optovue Inc., Fremont, CA). Recording and analysis techniques were published previously (1–3).

Animals. To define the structural and functional consequences of XLPRA1 and XLPRA2 disease and set the stage for treatment and outcome assessment, we used wild-type (n = 17, ages 7–416 wk), XLPRA1 (n = 9, ages 7–156 wk), and XLPRA2 (n = 6, ages 8-144 wk) dogs for noninvasive imaging and ERG studies. For gene therapy, crossbred affected dogs were used (4, 5) (Tables S1 and S2). All procedures involving animals were performed in compliance with the Association for Research in Vision and Ophthalmology (ARVO) Statement for the Use of Animals in Ophthalmic and Vision Research and with Institutional Animal Care and Use Committee approval.

Therapeutic Transgene, Promoters, and Recombinant Adeno-Associated Virus Vector Production and Purification. The vector cDNA was a full-length human *RPGR*ORF15 clone, based on the sequence published by Alan Wright and colleagues (variant C; NM_001034853) (6). This construct contains exons 1-ORF15 and was generated using three-way ligation by step-wise amplifying exons 1-part of 15b (nucleotides 169–1990) from human lymphocytes and 1991–3627 from human genomic DNA. An internal restriction enzyme site Nde1 (CATATG) was created by site-directed mutagenesis at residue 1993 (A>T). These fragments were then cloned in BamHI and XhoI sites in pBluescript, propagated in *E. coli* Stbl4, and sequence-verified at the University of Michigan DNA sequencing core facility.

The human G protein-coupled receptor protein kinase 1 (hGRK1) promoter was used to primarily control rod expression in the dog retina at a therapeutic concentration of 10^{11} vg/ml; higher concentrations (10^{13}) result in expression in some cones, but with adverse retinal effects (7). Expression in both rods and cones was regulated by 235 bp of the human IRBP promoter (8) that contains the important *cis*-acting element identified in the mouse proximal promoter (9); vectors with this promoter result in GFP expression in both rods and cones in a dose- and time-dependent manner (Fig. S5). Vector DNA sequences were confirmed for accuracy before vector production. The two-plasmid cotransfection method was used to produce the AAV2/5 vector (10). Viral particles were titered and resuspended in balanced salt solution (BSS; Alcon Laboratories, Fort Worth, TX) containing 0. 014% Tween 20 at a concentration of 1.5×10^{11} viral vector genomes per mL (vg/ml). Sterility and the lack of endotoxin were confirmed in the final product.

Subretinal Injections and Posttreatment Management. Subretinal injections were performed under general anesthesia as previously published (7, 11). The volume injected was dependent on age/eye size: 70 μl and 150 μl, respectively, at 5 and 28 wk of age, with the therapeutic vector injected in the right eye, and BSS injected in the left. At the time of the injection, the location and extent of the subretinal blebs were recorded on fundus photographs or schematic fundus illustrations; in all cases, the blebs flattened and the retina reattached within 24 h. Failed subretinal injection that refluxed into the vitreous was found in one dog that was maintained throughout the study to determine potential therapeutic efficacy and/or ocular complications by the intravitreal route.

Clinical Assessment and in Vivo Retinal Imaging. Ophthalmic examinations were conducted throughout the injection-termination time interval. *En face* and retinal cross-sectional imaging was performed (1–3, 12, 13) with the dogs under general anesthesia. Overlapping *en face* images of reflectivity with near-infrared illumination (820 nm) were obtained with Heidelberg Retina Angiogram (HRA) units (HRA2 or Spectralis HRA or Spectralis HRA+OCT, Heidelberg, Germany) with 30° and 55° diameter lenses to delineate fundus features such as optic nerve, retinal blood vessels, boundaries of injection blebs, retinotomy sites, and other local changes. Custom programs (MatLab 6.5; The MathWorks, Natick, MA) were used to digitally stitch individual photos into a retina-wide panorama. In a subset of eyes, short-wavelength (488 nm) illumination was used to delineate the boundary of the tapetum and pigmented RPE. Spectral-domain optical coherence tomography (SD-OCT) was performed with linear and raster scans (RTVue-100; Optovue, Inc., Fremont, CA; or Spectralis HRA+OCT, Heidelberg, Germany). Linear scans were placed across regions or features of interest such as bleb boundaries in order to obtain highly resolved local retinal structure. The bulk of the cross-sectional retinal information was obtained from overlapping raster scans covering large regions of the retina. Raster scans covered retinal regions of either 6 × 6 mm [101 lines of 513 longitudinal reflectivity profiles (LRPs) each, no averaging, Optovue] or 9 × 6 mm (49 lines of 1536 LRPs each, averaging 8–10, Spectralis).

Post-acquisition processing of OCT data was performed with custom programs (MatLab 6.5; The MathWorks, Natick, MA). For retina-wide topographic analysis, integrated backscatter intensity of each raster scan was used to locate its precise location and orientation relative to retinal features visible on the retina wide mosaic formed by NIR reflectance images. Individual LRPs forming all registered raster scans were allotted to regularly spaced bins (1° × 1°) in a rectangular coordinate system centered at the optic nerve; LRPs in each bin were aligned and averaged. Intraretinal peaks and boundaries corresponding to histologically definable layers were segmented semiautomatically with manual override using both intensity and slope information of backscatter signal along each LRP. Specifically, the retina–vitreous interface, outer plexiform layer (OPL), outer limiting membrane (OLM), signal peak near the inner/outer segment (IS/OS) junction, and the retinal pigment epithelium (RPE) were defined. In the superior retina of the dog, backscatter from the tapetum forms the highest intensity peak, and RPE and IS/OS peaks are located vitreal to the tapetal peak. ONL thickness was defined from the sclerad transition of the OPL to the OLM, and ONL thickness topography was calculated. In addition, the topography of IS/OS backscatter intensity was calculated by first measuring the mean backscatter intensity within ±8 μm of the IS/OS peak and then normalizing this value by the mean backscatter intensity of the first 75 μm of retina sclerad to the retina-vitreous interface. For all topographic results, locations of blood vessels, optic nerve head and bleb boundaries were overlaid for reference. Further quantitative comparisons were achieved by sampling the ONL thickness of a 10° wide band along the vertical meridian crossing the optic nerve head.

Electroretinography. Dogs were dark-adapted overnight, premedicated, and anesthetized as described (14, 15). Pupils were dilated with atropine (1%), tropicamide (1%), and phenylephrine (10%). Pulse rate, oxygen saturation, and temperature were monitored. Full-field ERGs were recorded with Burian–Allen (Hansen Ophthalmics, Iowa City, IA) contact lens electrodes and a computer-based system. White flashes of low-energy (10 μs duration; 0.4 log scotopic-candelas (scot-cd)·s·m^{-2}; scot-cd·s·m^{-2}) and high-energy (1 ms duration; 3.7 log scot-cd·s·m^{-2}) were used under dark-adapted and light-adapted (1.5 log cd·m^{-2} at 1 Hz stimulation, 0.8 log cd·m^{-2} at 29 Hz stimulation) conditions. Leading edges of high-energy flash responses were measured at the fixed time point of 4 ms (16) to quantify retinal function dominated by the rod photoreceptors, and the peak-to-peak amplitude of the low-energy flashes at 29 Hz were measured to quantify retinal function dominated by the cone photoreceptors. Assessment of visual behavior using qualitative or quantitative measures was not performed in treated animals because, at the disease stages studied, both mutant strains (untreated) retain sufficient rod and cone visual function that they are not distinguishable from normal.

Tissue Processing and Morphologic Assessment. Dogs were euthanatized by intravenous injection of euthanasia solution (Euthasol; Virbac, Ft. Worth, TX), and the globes were enucleated, fixed, and processed as previously described (4). Serial 10-μm-thick retinal cryosections that encompassed treated and nontreated regions were cut (~700 per retina), and a subset were stained with H&E; vascular landmarks were used to place the section on the *en face* confocal scanning laser ophthalmoscope (cSLO) images and subsequent *en face* ONL maps. Immunohistochemistry was done in adjacent sections with antibodies directed against rod opsin, human cone arrestin (LUMIf; 1/10,000 provided by Cheryl Craft, University of Southern California), R/G-opsin, RIBEYE/CtBP2, PKCα, Goα, calbindin, neurofilament (NF200 kDa), and GFAP to examine the expression of molecular markers in treated and nontreated areas (4, 17). As well, an antibody directed at the C-terminal domain of human RPGR (18) was used to identify the therapeutic transgene product in treated eyes. The antigen–antibody complexes were visualized with fluorochrome-labeled secondary antibodies (Alexa Fluor, 1:200; Molecular Probes, Eugene, OR) with DAPI to label cell nuclei, and digital images were taken (Spot 4.0 camera; Diagnostic Instruments, Sterling Heights, MI) and imported into a graphics program (Photoshop; Adobe, Mountain View, CA) for display.

1. Jacobson SG, et al. (2009) Disease boundaries in the retina of patients with Usher syndrome caused by MYO7A gene mutations. *Invest Ophthalmol Vis Sci* 50: 1886–1894.
2. Jacobson SG, et al. (2008) Photoreceptor layer topography in children with leber congenital amaurosis caused by RPE65 mutations. *Invest Ophthalmol Vis Sci* 49: 4573–4577.
3. Jacobson SG, et al. (2011) Human retinal disease from AIPL1 gene mutations: foveal cone loss with minimal macular photoreceptors and rod function remaining. *Invest Ophthalmol Vis Sci* 52:70–79.
4. Beltran WA, Hammond P, Acland GM, Aguirre GD (2006) A frameshift mutation in RPGR exon ORF15 causes photoreceptor degeneration and inner retina remodeling in a model of X-linked retinitis pigmentosa. *Invest Ophthalmol Vis Sci* 47:1669–1681.
5. Zeiss CJ, Acland GM, Aguirre GD (1999) Retinal pathology of canine X-linked progressive retinal atrophy, the locus homologue of RP3. *Invest Ophthalmol Vis Sci* 40:3292–3304.
6. Vervoort R, et al. (2000) Mutational hot spot within a new RPGR exon in X-linked retinitis pigmentosa. *Nat Genet* 25:462–466.
7. Beltran WA, et al. (2010) rAAV2/5 gene-targeting to rods:dose-dependent efficiency and complications associated with different promoters. *Gene Ther* 17:1162–1174.
8. al-Ubaidi MR, et al. (1992) Bilateral retinal and brain tumors in transgenic mice expressing simian virus 40 large T antigen under control of the human interphotoreceptor retinoid-binding protein promoter. *J Cell Biol* 119:1681–1687.
9. Boatright JH, et al. (1997) A major cis activator of the IRBP gene contains CRX-binding and Ret-1/PCE-I elements. *Mol Vis* 3:15.
10. Zolotukhin S, et al. (1999) Recombinant adeno-associated virus purification using novel methods improves infectious titer and yield. *Gene Ther* 6:973–985.
11. Komáromy AM, et al. (2010) Gene therapy rescues cone function in congenital achromatopsia. *Hum Mol Genet* 19:2581–2593.
12. Cideciyan AV, et al. (2005) In vivo dynamics of retinal injury and repair in the rhodopsin mutant dog model of human retinitis pigmentosa. *Proc Natl Acad Sci USA* 102:5233–5238.
13. Alemán TS, et al. (2007) Inner retinal abnormalities in X-linked retinitis pigmentosa with RPGR mutations. *Invest Ophthalmol Vis Sci* 48:4759–4765.
14. Acland GM, et al. (2001) Gene therapy restores vision in a canine model of childhood blindness. *Nat Genet* 28:92–95.
15. Kijas JW, et al. (2002) Naturally occurring rhodopsin mutation in the dog causes retinal dysfunction and degeneration mimicking human dominant retinitis pigmentosa. *Proc Natl Acad Sci USA* 99:6328–6333.
16. Acland GM, et al. (2005) Long-term restoration of rod and cone vision by single dose rAAV-mediated gene transfer to the retina in a canine model of childhood blindness. *Mol Ther* 12:1072–1082.
17. Beltran WA, Acland GM, Aguirre GD (2009) Age-dependent disease expression determines remodeling of the retinal mosaic in carriers of RPGR exon ORF15 mutations. *Invest Ophthalmol Vis Sci* 50:3985–3995.
18. Khanna H, et al. (2005) RPGR-ORF15, which is mutated in retinitis pigmentosa, associates with SMC1, SMC3, and microtubule transport proteins. *J Biol Chem* 280: 33580–33587.

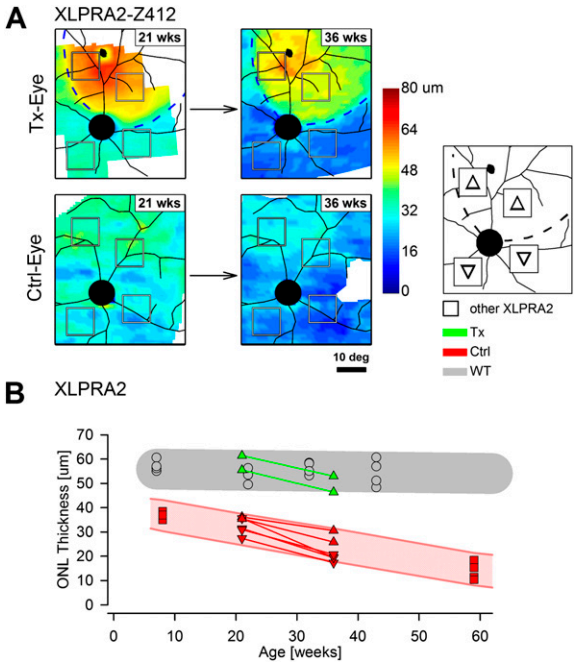

Fig. S1. Longitudinal followup of ONL thickness changes in treated and control eyes of XLPRA2-Z412. (*A*) ONL topography of the two eyes of the XLPRA2 dog Z412 at 21 and 36 wk of age. At 5 wk of age, the treated eye received subretinal AAV2/5-*hIRPB-hRPGR* vector injection, creating a transient superior-nasal bleb (dashed lines), and the control eye received a BSS injection. Squares denote the two regions of interest chosen within the AAV bleb boundary and two regions outside the bleb boundary. ONL thickness is mapped to a pseudocolor scale; white represents "no data." (*B*) Quantitative analysis of the ONL thickness from the eyes of Z412 (red and green triangles) compared with other XLPRA2 dogs (red squares) and wild-type controls. Pink region is drawn to encompass all available XLPRA2 data and gray region all available wild-type data. Symbols and colors are depicted in key. Longitudinal measurements in the same eye are represented with connected lines (*B*).

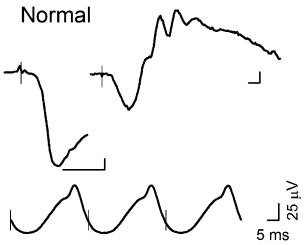

Fig. S2. ERGs in a representative normal (wild type) dog (age = 40 wk) to compare with the waveforms shown in Fig. 2*D*. Upper-left waveform is the leading edge of the photoresponse driven by rod photoreceptor activation, and the upper-right waveform is the b-wave dominated by rod bipolar cells; both were recorded under dark-adapted conditions. The lower waveform is 29-Hz flicker responses dominated by cone function recorded under light-adapted conditions. Black vertical lines show the timing of flash onset. All calibrations are 5 ms and 25 μV.

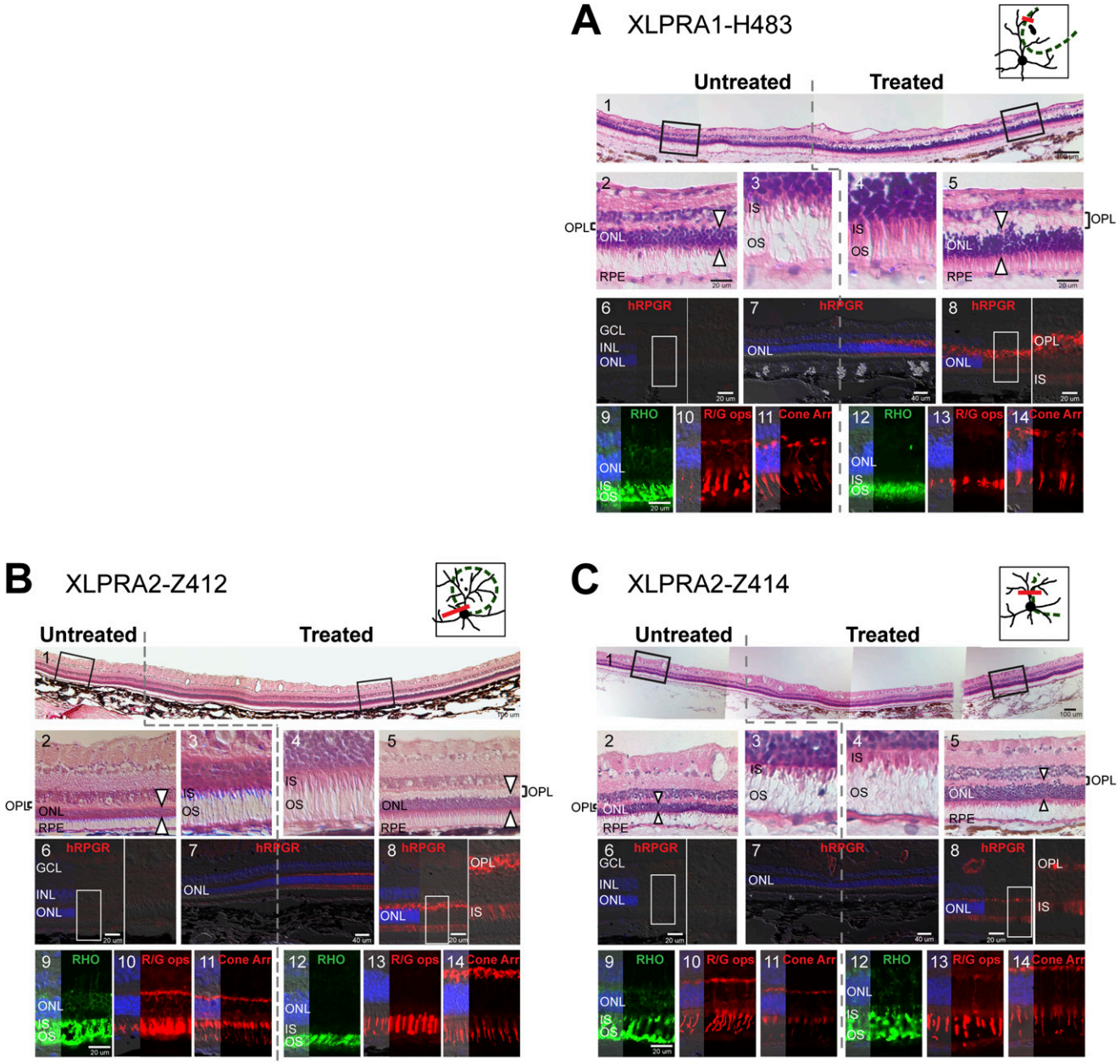

Fig. S3. Gene replacement therapy rescues photoreceptors in XLPRA. (*A*) XLPRA1 dog treated with *AAV2/5-hIRPB-hRPGR* at 28 wk of age and tissues collected at 77 wk. (*B* and *C*) XLPRA2 dogs treated with (*B*) AAV2/*5-hIRPB-hRPGR* or (*C*) AAV2/*5-hGRK1-hRPGR* at 5 wk of age and tissues collected at 38 wk. The schematic drawings for *A*–*C* illustrate the treatment area (dashed green lines) and the location of the region (red line) illustrated in the sections. (1) Representative H&E-stained cryosection at the nontreated/treated junction (vertical dashed line). Boxed areas are illustrated at higher magnification below (2–5). Photoreceptor density is decreased in the nontreated region, and both ONL (white arrowheads) and OPL are narrowed; rod and cone IS are short, and OS sparse. In treated regions, the number of photoreceptors is increased and their structure is normal (*A*, 4; *B*, 4) or improved (*C*, 4), resulting in thicker ONL and preserved OPL. (6–8) Expression of hRPGRORF15 in treated areas decreases in the transition zone and is absent elsewhere. Protein is present in rod and cone inner segments and synaptic regions. Dog Z414 shows the lowest level of expression. (9, 10, 12, and 13) Rod (RHO) and red/green cone opsins (R/G ops) are mislocalized in untreated regions with label in the IS, ONL, and synaptic terminals. Treated areas show normal localization to the OS in dogs treated with AAV2/*5-hIRPB-hRPGR* vector, but partial mislocalization persists in Z414. (11 and 14) Preservation of normal cone structure in treated areas is clearly shown with cone arrestin (Cone Arr) labeling. GCL, ganglion cell layer; INL, inner nuclear layer; IS, inner segments; ONL, outer nuclear layer; OPL, outer plexiform layer; OS, outer segments; RPE, retinal pigment epithelium. Calibration marker = 20 μm for main panels.

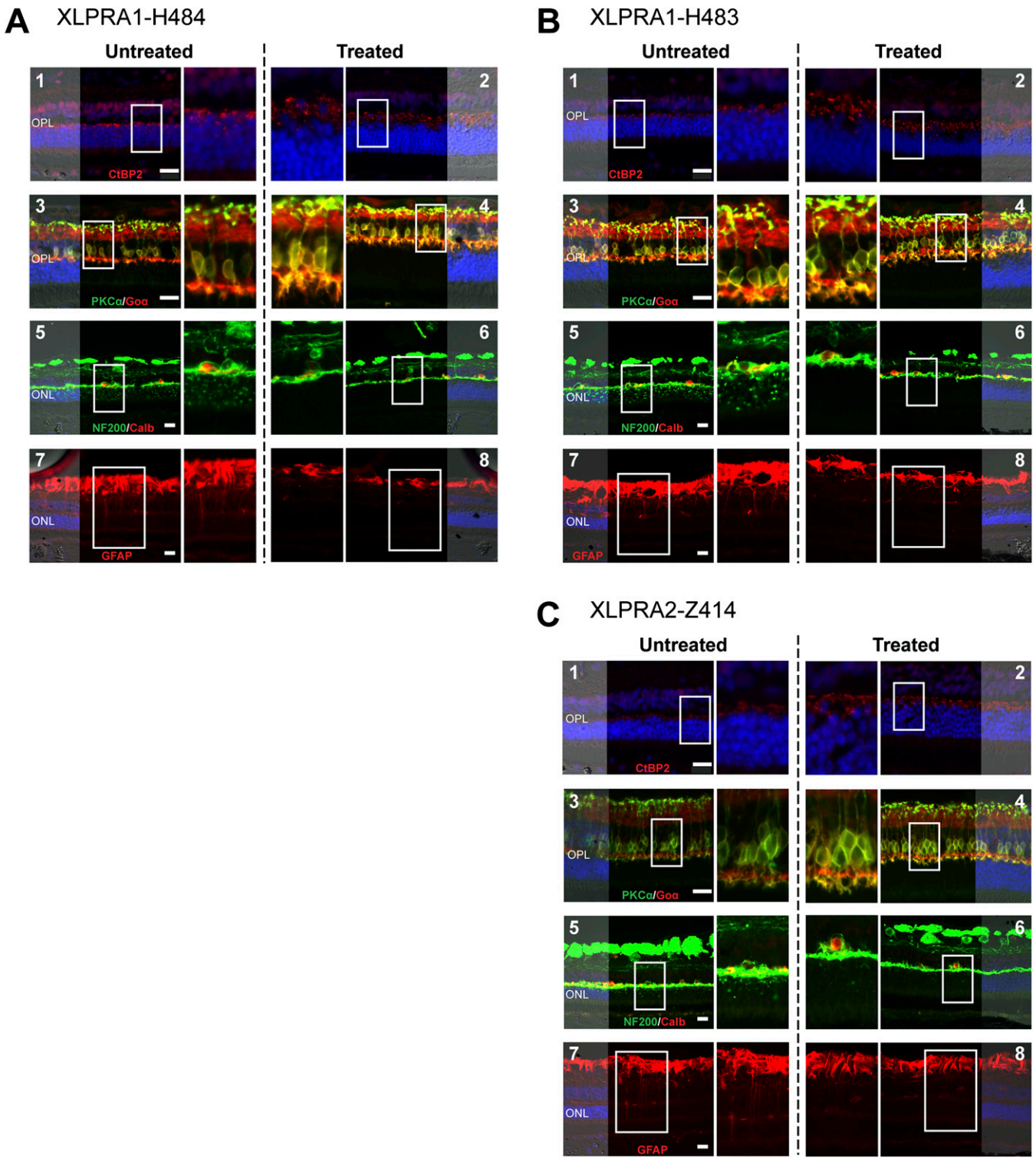

Fig. S4. Successful gene therapy rescues retinal remodeling in XLPRA. (*A* and *B*) XLPRA1 dogs treated with *AAV2/5-hIRPB-hRPGR* at 28 wk of age and terminated at 77 wk. (*C*) XLPRA2 dog treated with AAV2/*5-hGRK1-hRPGR* at 5 wk of age and terminated at 38 wk. (1 and 2) Immunolabeling with CtBP2/RIBEYE shows a reduced number of photoreceptor synaptic ribbons in the untreated areas; in treated areas, the density of synaptic ribbons is normal, thus contributing to the preservation of the OPL thickness. (3 and 4) Coimmunolabeling of rod bipolar (PKCα) and ON bipolar cells (Goα) shows retraction of dendrites in untreated areas, whereas denditic arborizations are preserved in treated regions. (5 and 6) Coimmunolabeling of the inner retina with neurofilament 200 kDa (NF200) and calbindin (Calb) antibodies is normal in both untreated and treated regions, but punctate NF200 staining is seen in the ONL of untreated areas. Treated areas show absence of NF200 labeling in the ONL of dogs that received the AAV2/*5-hIRPB-hRPGR* vector (*A*, 6; *B*, 6), but rare staining is seen in the ONL of dog Z414 treated with the AAV2/*5-hGRK1-hRPGR* vector (*C*, 6). (7 and 8) GFAP immunolabeling of Müller cell radial extensions is found only in untreated areas, whereas no reactive Müller cells are seen in the treated regions.

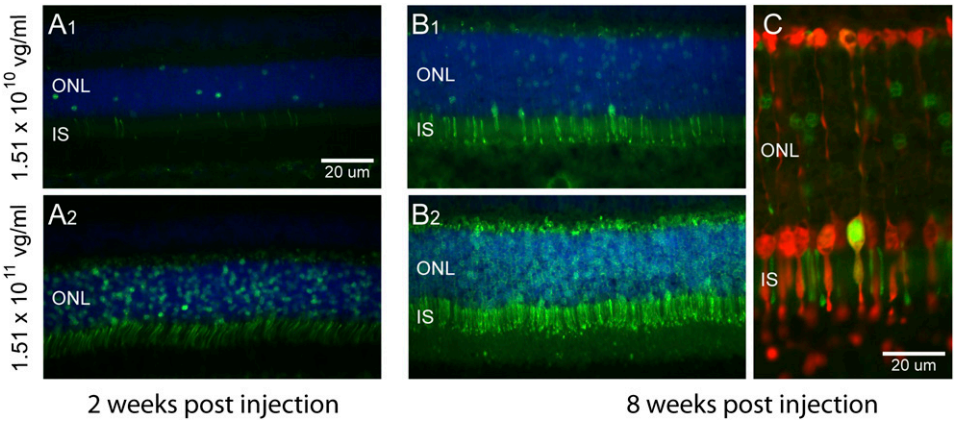

Fig. S5. AAV2/5 vector with hIRBP promoter targets expression to rods and cones. Native GFP fluorescence (green) in normal canine retina 2 and 8 wk following subretinal injection of *AAV2/5-hIRBP-hGFP*. Injections (150 μL) of two vector titers were used. GFP fluorescence in photoreceptors is present by 2 wk (*A*1 and *A*2) and is increased at 8 wk (*B*1 and *B*2). Expression is found in both rods and cones as confirmed by colocalization with cone arrestin in retinas treated with lower vector dose that results in fewer cones transduced (*C*). More photoreceptors are labeled at the higher dose, and expression is sustained during the 8-wk treatment period.

Table S1. Treatment outcomes for *RPGR* gene augmentation therapy

Genotype of animal/eye	Age (wk)*		Agent injected[†]	Treatment outcomes							
				OCT		ERG[¶]		Morphology/ IHC			hRPGR expression[‡‡]
	Begin	End		ONL[‡]	IS/OS[§]	Rod	Cone	PR[‖]	OPL**	Inner retina[††]	
XLPRA1											
H484/RE	28	77	*hIRBP-hRPGR*	+	+	+	+	N	N	N	+3
H484/LE			BSS	—	—			D	D	D	-
H483/RE	28	77	*hIRBP-hRPGR*	+	+	—	—	N	N	N	+2
H483/LE			BSS	—	—			D	D	D	-
XLPRA2											
Z412/RE	5	38	*hIRBP-hRPGR*	+	+	+	+	N	N	N	+2
Z412/LE			BSS	—	—			D	D	D	-
Z414/RE	5	38	*hGRK1-hRPGR*	—	+	+	+	P	P	P	+1
Z414/LE			BSS	—	—			D	D	D	-
Z413/RE	5	38	*hGRK1-hRPGR* (*intravitreal control*)	ND	ND	ND	ND	D	D	D	-

BSS, balanced salt solution; D, diseased; LE, left eye; N, normal rescue; ND, not done; P, partial rescue; RE, right eye; +, positive treatment outcome; —, no response to treatment.

*The span of ages (in weeks) from treatment to termination.

[†]Subretinal injections with a volume of 70 μL at 5 wk of age and 150 μL at 28 wk. AAV2/5 vector injections had a titer of 1.5×10^{11} vg/mL. Dog Z413 had 70 μL injected into the vitreous and served as control.

[‡]Existence of a region of retained outer nuclear layer (ONL) within the injection bleb compared with outside the bleb as measured by optical coherence tomography (OCT).

[§]Existence of a region of higher inner segment/outer segment (IS/OS) reflectivity within the injection bleb compared with outside the bleb as measured by OCT.

[¶]Interocular asymmetry of the rod- or cone-dominated electroretinogram (ERG) amplitudes.

[‖]Photoreceptors (PR). Structure of rods, cones, and outer nuclear layer in treated vs. untreated regions and reversal of rod and cone opsin mislocalization.

**Outer plexiform layer (OPL). Pre- and postsynaptic terminal structures, including presence of normal elongated bipolar dendrites as determined by immunohistochemistry (IHC) using antibodies that label photoreceptor synaptic terminals and bipolar cells.

[††]Reversal/prevention of inner retinal remodeling.

[‡‡]hRPGR expression in treated area determined with a C-terminal antibody. Labeling limited to rods and cones and graded as: - (no label), +1 (weak), +2 (moderate), and +3 (intense).

Table S2. Treatment failures or complications in *RPGR* gene therapy with AAV2/5 vectors

	Age (wk) begin/end	Promoter-transgene (no. of eyes)	Vector titer (vg/mL)	Outcome	
				Rescue	Complications (no. of eyes)
XLPRA1 augmentation	26–28/31–37	*mOP-cRPGR* (1)	1.5×10^{11}	No	Multifocal rosettes (1)
		hIRBP-HiscRPGR (4)	1.5×10^{11}	No	Multifocal rosettes (4)
		hGRK1-hRPGR (1)	1.5×10^{11}	*	Small retinal detachments (1)
XLPRA2 knockdown	5–22/20–39	*CBA-GFP-H1-siRNA3* (1)	$2.8–2.9 \times 10^{11}$	No	None
		CBA-GFP-H1-siRNA5 (1)		No	None
		CBA-GFP-H1-siRNA5 (1)		No	None
		CBA-GFP-H1-siRNA5 (2)		No	None
XLPRA2 knockdown and augmentation	5/22	*hIRBP-cRPGR_HT-H1-siRNA5* (3)	1.5×10^{10}	No	Multifocal rosettes (2); none (1)
		hIRBP-cRPGR_HT-H1-siRNA5 (2)-IV	1.5×10^{11}	No	None (2)

Previous hypotheses about XLPRA2 being due to a toxic gain of function (1) led to attempts to down-regulate mutant *RPGR* expression to improve the disease. Two knockdown reagents, *shRNA3* and *shRNA5*, which were effective in downregulating canine *RPGR* expression in vitro, were used, but there was no rescue. Simultaneous replacement of *RPGR* used a single viral construct that combined *shRNA5* and a resistant abbreviated (2) canine *RPGR* cDNA that had a 5′ 6xHis tag. Subretinal treatment with high vector titer resulted in no efficacy and retinal toxicity. Similar retinal toxicity was observed by augmentation alone with the abbreviated canine *RPGR* cDNA without the His tag. *c*, canine; *CBA*, chicken beta actin promoter (3); *h*, human; IV, intravitreal control; *mOP*, minimal opsin promoter.

*Mild and nonuniform hRPGR expression in treatment area, partial recovery of opsin mislocalization. Photoreceptor rescue was not interpretable because of the retinal detachments, and early termination secondary to these complications.

1. Zhang Q, et al. (2002) Different RPGR exon ORF15 mutations in Canids provide insights into photoreceptor cell degeneration. *Hum Mol Genet* 11:993–1003.
2. Hong DH, Pawlyk BS, Adamian M, Sandberg MA, Li T (2005) A single, abbreviated RPGR-ORF15 variant reconstitutes RPGR function in vivo. *Invest Ophthalmol Vis Sci* 46:435–441.
3. Beltran WA, et al. (2010) rAAV2/5 gene-targeting to rods: Dose-dependent efficiency and complications associated with different promoters. *Gene Ther* 17:1162–1174.